EUROPEAN HEMATOLOGY ASSOCIATION
haematologica
Journal of the European Hematology Association

New molecular and therapeutic insights into canine diffuse large B cell lymphoma elucidates the role of the dog as a model for human disease

by Luca Aresu, Serena Ferraresso, Laura Marconato, Luciano Cascione, Sara Napoli, Eugenio Gaudio, Ivo Kwee, Chiara Tarantelli, Andrea Testa, Chiara Maniaci, Alessio Ciulli, Petra Hillmann, Thomas Bohnacker, Matthias P. Wymann, Stefano Comazzi, Massimo Milan, Fulvio Riondato, Giulia Dalla Rovere, Mery Giantin, Diana Giannuzzi, and Francesco Bertoni

Haematologica 2018 [Epub ahead of print]

Citation: Luca Aresu, Serena Ferraresso, Laura Marconato, Luciano Cascione, Sara Napoli, Eugenio Gaudio, Ivo Kwee, Chiara Tarantelli, Andrea Testa, Chiara Maniaci, Alessio Ciulli, Petra Hillmann, Thomas Bohnacker, Matthias P. Wymann, Stefano Comazzi, Massimo Milan, Fulvio Riondato, Giulia Dalla Rovere, Mery Giantin, Diana Giannuzzi, and Francesco Bertoni. New molecular and therapeutic insights into canine diffuse large B cell lymphoma elucidates the role of the dog as a model for human disease. Haematologica. 2018; 103:xxx doi:10.3324/haematol.2018.207027

New molecular and therapeutic insights into canine diffuse large B cell lymphoma elucidates the role of the dog as a model for human disease

Luca Aresu [1*], Serena Ferraresso [2], Laura Marconato [3], Luciano Cascione [4,5], Sara Napoli [4], Eugenio Gaudio [4], Ivo Kwee [4,5,6], Chiara Tarantelli [4], Andrea Testa [7], Chiara Maniaci [7,8], Alessio Ciulli [7], Petra Hillmann [9], Thomas Bohnacker [10], Matthias P. Wymann [10], Stefano Comazzi [11], Massimo Milan [2], Fulvio Riondato [1], Giulia Dalla Rovere [2], Mery Giantin [2], Diana Giannuzzi [2], Francesco Bertoni [4*]

[1] Dipartimento di Scienze Veterinarie, Università degli Studi di Torino, Torino, Italy;
[2] Dipartimento di Biomedicina Comparata e Alimentazione, Università degli Studi di Padova, Padova, Italy;
[3] Centro Oncologico Veterinario, Sasso Marconi, Italy;
[4] Università della Svizzera italiana (USI), Institute of Oncology Research (IOR), Bellinzona, Switzerland;
[5] Swiss Institute of Bioinformatics (SIB), Lausanne, Switzerland;
[6] Dalle Molle Institute for Artificial Intelligence (IDSIA), Manno, Switzerland;
[7] Division of Biological Chemistry and Drug Discovery, School of Life Sciences, University of Dundee, Dundee, Scotland, United Kingdom;
[8] Department of Chemistry, Chemistry Research Laboratory, University of Oxford, Oxford, England, United Kingdom;
[9] PIQUR Therapeutics AG, Basel, Switzerland;
[10] Department of Biomedicine, University of Basel, Basel, Switzerland;
[11] Dipartimento di Medicina Veterinaria, Università degli Studi di Milano, Milano, Italy.

***Co-corresponding authors:**
-Prof. Luca Aresu, Dipartimento di Scienze Veterinarie, Università degli Studi di Torino, Largo Braccini 2, 10095 Grugliasco (TO), Italy. Phone: +390116708893; e-mail: luca.aresu@unito.it
-Dr Francesco Bertoni, Università della Svizzera italiana, Institute of Oncology Research, via Vincenzo Vela 6, 6500 Bellinzona, Switzerland. Phone: +41918200367; e-mail: frbertoni@mac.com.

Financial Support
SIR (Scientific Independence of Young Researchers) 2014, Ministero dell'Istruzione, dell'Universita' e della Ricerca (Number RBSI14EDX9) (to LA) and the Gelu Foundation (to FB).

Diffuse large B-cell lymphoma (DLBCL) is the commonest lymphoma both in humans and in dogs. [1]. Due to spontaneously high incidence, complex genetics interplay, aggressive clinical course, elevated frequency and the presence of an intact immune system, dogs with lymphoma are considered as an ideal comparative model for drug development for human lymphomas [1]. The BCL2 inhibitor venetoclax and the BTK inhibitors ibrutinib and acalabrutinib are examples of drugs that benefited of such model [2-4]. Clinical heterogeneity of canine DLBCL (cDLBCL) is known and early insights on its biologic and molecular mechanisms, revealing similarities with the human counterpart, have been reported, but a genomic characterization of this tumor has never been provided. Furthermore, a complete understanding of the molecular mechanisms driving cDLBCL pathogenesis is necessary to more accurately take advantage of this comparative model and, also, to improve the clinical outcome of the dogs. In this study, we report the first large integrated analysis with transcriptome sequencing, methylation genome wide analysis, copy number variation (CNV) analysis and clinical outcome in cDLBCLs to comprehensively define the molecular mechanisms of this tumor and to better define its use in comparative medicine.

We first compared the transcriptome obtained via RNA-Seq in 50 cDLBCLs versus RNA-Seq data of normal follicular B-cells derived from lymph nodes of 11 healthy dogs (*Online Supplementary Table S1; Online Supplementary Methods*). Transcripts higher in cDLBCLs than in controls were significantly enriched of genes coding for proteins involved in the B-cell receptor (BCR), MYC signaling, PI3K/AKT/mTOR pathway, DNA replication, and cell cycle (*Online Supplementary Figure S1*). Genes coding for proteins involved in the NF-kB pathway (CD79, CD19, SYK, LYN, CARD11, BCL10, BTK, TRAF6, MYD88, NFKB2, TLR7, TLR9) were also differentially expressed (*Figure 1*). The aberrant expression of these genes might contribute to enhance proliferation and protection from apoptosis of B-cells by stimulating NF-κB activity. A similar mechanism is described in human ABC-DLBCL, characterized by a constitutive activation of NF-κB due to mutations in multiple genes belonging to this pathway subgroup [5]. These data fit with the reported frequent inactivation of the NF-κB negative regulator TRAF3 in canine B-cell lymphomas [6], and the anti-tumor activity of BTK inhibitors, specifically active in the human ABC DLBCL subtype and experimentally used in canine B-cell lymphomas [3, 4].

The protein encoding gene LIN28B appeared as the most upregulated transcript in tumors. While LIN28B does not seem to be a relevant gene for human DLBCL, it is involved in the activation of the NF-kB pathway and of MYC in different human and mouse tumor models and its overexpression causes murine peripheral T-cell lymphomas [7]. We took advantage of the CLBL-1 cell line, the only *in vitro* model available of cDLBCL, which showed a profile similar to cDLBCL clinical specimens, with LIN28B as the most overexpressed gene compared to normal lymph nodes (*Online Supplementary Table S3*). LIN28B silencing using LNA modified-siRNAs led to a reduction in the cell-proliferation compared to the negative control (*Online Supplementary Figure S2*), opening new therapeutic target perspectives at least in cDLBCL.

The integration of CNVs data and transcriptome showed an association in 320 genes. A total of 239 genes were located in regions of gains and simultaneously overexpressed, while 81 genes were downregulated and mapped in regions of deletions (*Online Supplementary Table S4*). The gains of the entire Chr 13 and 31 and losses of Chr 14 were the most frequent aberrations, occurring in >20% of the cases (*Online Supplementary Figure S3*). Survival analysis showed a trend for longer OS and EFS in dogs affected by this Chr 13 aberration versus the remaining animals (P=0.134). A series of additional CNVs, such as gains in Chr 4, 27 and loss in Chr 28, were observed in at least two dogs (Figure S2).

A genome-wide NGS-based methylation analysis, previously never performed in canine lymphomas, identified differentially methylated regions (DMRs) between cDLBCLs and the normal follicular B-cells (*Online Supplementary Table S4; Online Supplementary Figure S4-5*). In accordance with RNA-Seq data, genes that presented a reduced degree of promoter methylation in cDLBCLs were enriched of transcripts involved in cytokine/cytokine receptor interaction, BCR and JAK/STAT signaling. Genes participating to calcium signaling, cytoskeleton, Hedgehog/Wnt signaling and metabolism more commonly presented an increased promoter methylation in neoplastic cells than in normal B-cells and were also down-regulated (*Online Supplementary Table S4*). In line with our previous study [8], the latter observed increased promoter methylation sustains the evaluation of hypomethylating agents in the treatment of cDLBCL.

Unsupervised clustering of RNA-Seq data separated cDLBCLs from normal follicular B-cells (*Figure 2A*) and identified two distinct subgroups within the tumors (*Figure 2B*). The two groups did not overlap with the human GCB and ABC DLBCL subtypes or the DLBCL consensus clusters [5], but they were associated with different OS (278 vs 150 days, *P*<0.01) and EFS (179 vs 113 days, *n.s*) (*Figure 2C-D*). Tumors belonging to the group with worse prognosis were characterized by a higher expression of transcripts coding for proteins involved in apoptosis, JAK/STAT signaling, microenvironment, inflammatory response and P53 pathway (*Online Supplementary Table S5*). In particular, dogs with the poorest outcome presented a signature largely defined by markers of T-cell-mediated immune responses, with a higher expression of transcripts involved in T-cells and macrophages regulation (CD163, CD96, PD-1, PDL-1, CTLA4, CD8a, CD4), as also shown by an enrichment of gene expression signatures of immune-inhibitory molecules (*Online Supplementary Figure S6*), and genes associated with ATP-binding cassette transporter. The two DLBCL clusters were also sustained by methylation and CNV differences (*Online Supplementary Figure S7).* Cases with inferior outcome presented a higher degree of promoter methylation (P<0.005), and a higher number of aberrations (*P*<0.01) compared to the remaining, but no equivalent to the human 9p24 amplification associated with expression of PD-L1, which could be mainly sustained by the observed activation of JAK/STAT pathway.

We first validated the pattern of expression of PDL-1, PD-1, CTLA-4 and CD5 by immunohistochemistry (*Online Supplementary Figure S8*). All the 25 samples belonging to the poor outcome group were strongly positive for PDL-1 and CTLA-4 (TPS higher than 50%), while cases of the other cluster were completely negative (n=5, 20%) or weakly positive (TPS between 1% and 40%; n=20, 80%). The same cases also presented a higher number of PD-1 and CD5 positive cells (higher or lower than 20 for HPF). We then analyzed an independent series of 44 cDLBCLs, all treated with CHOP plus vaccine [9]. PDL-1 and PD-1 stainings were positive in 21 (48%) and 25 cases (57%), respectively, and conferred inferior outcome (*Figure 2E-F*). CTLA-4 and CD5 expression occurred in 18 (41%) and 22 cases (50%) but were not associated with clinical outcome. In a multivariate analysis including bone marrow infiltration and substage, PD-L1 and PD-1 maintained their prognostic impact on OS, but not on EFS (*Online Supplementary Table S6*). The obtained results represent a strong basis towards the evaluation novel regimens based on immune-checkpoint inhibitors in canine lymphomas before moving to the human setting. Combination of immune checkpoint modulators with active vaccines [9] would be also worth of being explored.

Transcriptome data suggested potential therapeutic implications. First, cDLBCLs presented gene expression signatures suggestive of MYC activation and we assessed the BET inhibitor birabresib (MK-8628/OTX015) [10] and the BRD4 degrader MZ1 (alongside its inactive epimer cis MZ1) [11] for their capability to block the proliferation of the CLBL-1 [12]. Both drugs inhibited proliferation, although MZ1 was more potent (*Online Supplementary Figure S9A*), in accordance to data obtained in human DLBCL models [13]. Interestingly, MZ1 significantly down-regulated not only MYC, but also LIN28B (*Online Supplementary Figure S9B*). Second, also in agreement with a transcriptome study based on a small number of canine B-cell lymphomas [14], genes belonging to the PI3K/AKT/mTOR pathway and/or to gene expression signatures obtained in human DLBCL cell lines exposed to BCR inhibitors [15] were enriched in the transcripts expressed in cDLBCL and in the CLBL-1 (*Online Supplementary Figure S10*), we tested a dual PI3K/mTOR inhibitor bimiralisib (PQR309) and PI3K-delta inhibitor idelalisib. Both drugs were active in the CLBL-1 cell line with IC50 values of 150nM and 80nM, respectively (*Online Supplementary Figure S9C*). A xenograft model with CLBL-1 implanted in NOD-SCID mice showed that both bimiralisib and MZ1, given at the dose of 100 mg/kg, significantly affected tumor growth in comparison with the control group, with reduction in the tumor volume of 43% and 33% versus control on day 8 (*P* < 0.05) (*Online Supplementary Figure S9D*).

In conclusion, we identified deregulated pathways and individual transcripts providing therapeutic targets, including an immune-related signature affecting the outcome of a subgroup of cDLBCL. Our study provides a series of novel findings that allow a better understanding of cDLBCL as comparative model for human DLBCL but will also lead to improvements in the management of dogs in the veterinary clinical practice.

REFERENCES

1. Aresu L. Canine Lymphoma, More Than a Morphological Diagnosis: What We Have Learned about Diffuse Large B-Cell Lymphoma. Front Vet Sci. 2016;3:77.
2. Souers AJ, Leverson JD, Boghaert ER, et al. ABT-199, a potent and selective BCL-2 inhibitor, achieves antitumor activity while sparing platelets. Nat Med. 2013;19(2):202-208.
3. Harrington BK, Gardner HL, Izumi R, et al. Preclinical Evaluation of the Novel BTK Inhibitor Acalabrutinib in Canine Models of B-Cell Non-Hodgkin Lymphoma. PLoS One. 2016;11(7):e0159607.
4. Honigberg LA, Smith AM, Sirisawad M, et al. The Bruton tyrosine kinase inhibitor PCI-32765 blocks B-cell activation and is efficacious in models of autoimmune disease and B-cell malignancy. Proc Natl Acad Sci U S A. 2010;107(29):13075-13080.
5. Pasqualucci L, Dalla-Favera R. Genetics of diffuse large B-cell lymphoma. Blood. 2018;131(21):2307-2319.
6. Bushell KR, Kim Y, Chan FC, et al. Genetic inactivation of TRAF3 in canine and human B-cell lymphoma. Blood. 2015;125(6):999-1005.
7. Beachy SH, Onozawa M, Chung YJ, et al. Enforced expression of Lin28b leads to impaired T-cell development, release of inflammatory cytokines, and peripheral T-cell lymphoma. Blood. 2012;120(5):1048-1059.
8. Ferraresso S, Arico A, Sanavia T, et al. DNA methylation profiling reveals common signatures of tumorigenesis and defines epigenetic prognostic subtypes of canine Diffuse Large B-cell Lymphoma. Sci Rep. 2017;7(1):11591.
9. Marconato L, Frayssinet P, Rouquet N, et al. Randomized, placebo-controlled, double-blinded chemoimmunotherapy clinical trial in a pet dog model of diffuse large B-cell lymphoma. Clin Cancer Res. 2014;20(3):668-677.
10. Boi M, Gaudio E, Bonetti P, et al. The BET Bromodomain Inhibitor OTX015 Affects Pathogenetic Pathways in Preclinical B-cell Tumor Models and Synergizes with Targeted Drugs. Clin Cancer Res. 2015;21(7):1628-1638.
11. Zengerle M, Chan KH, Ciulli A. Selective Small Molecule Induced Degradation of the BET Bromodomain Protein BRD4. ACS Chem Biol. 2015;10(8):1770-1777.
12. Rutgen BC, Willenbrock S, Reimann-Berg N, et al. Authentication of primordial characteristics of the CLBL-1 cell line prove the integrity of a canine B-cell lymphoma in a murine in vivo model. PLoS One. 2012;7(6):e40078.
13. Tarantelli C, Ekeh H, Moscatello C, et al. Abstract A179: The BRD4 degrader MZ1 exhibits potent antitumoral activity in diffuse large B cell lymphoma of the activated B cell-like type. Mol Cancer Ther. 2018;17(1 Supplement):A179-A179.
14. Mooney M, Bond J, Monks N, et al. Comparative RNA-Seq and microarray analysis of gene expression changes in B-cell lymphomas of Canis familiaris. PLoS One. 2013;8(4):e61088.
15. Tarantelli C, Gaudio E, Arribas AJ, et al. PQR309 Is a Novel Dual PI3K/mTOR Inhibitor with Preclinical Antitumor Activity in Lymphomas as a Single Agent and in Combination Therapy. Clin Cancer Res. 2018;24(1):120-129.

Figure legends

Figure 1. Schematic representation of potential NFkB activation pathway obtained by RNA-seq analysis in cDLBCLs. Red, upregulated genes. Green, downregulated genes. Yellow, non-changing genes.

Figure 2. Unsupervised clustering of cDLBCLs RNA-Seq data identifies groups with different outcome. Multidimensional scaling (MDS) plot of all the samples demonstrated a clear separation between normal B-cells (green dots) and cDLBCLs (red dots) (a). Two cDLBCL subgroups (blue and red) were defined by hierarchical clustering (b). Kaplan-Meier plots of overall survival (c) and event free survival (d) of cDLBCLs grouped on the basis of RNA-seq profiling. Prognostic impact of PD-L1 tumor expression and PD-1 residual lymphocyte expression on overall survival and event free survival in cDLBCL: Kaplan-Meier plots of overall survival (e, g) and event free survival (f, h) based on immunohistochemical scores of PDL1 and PD1, respectively.

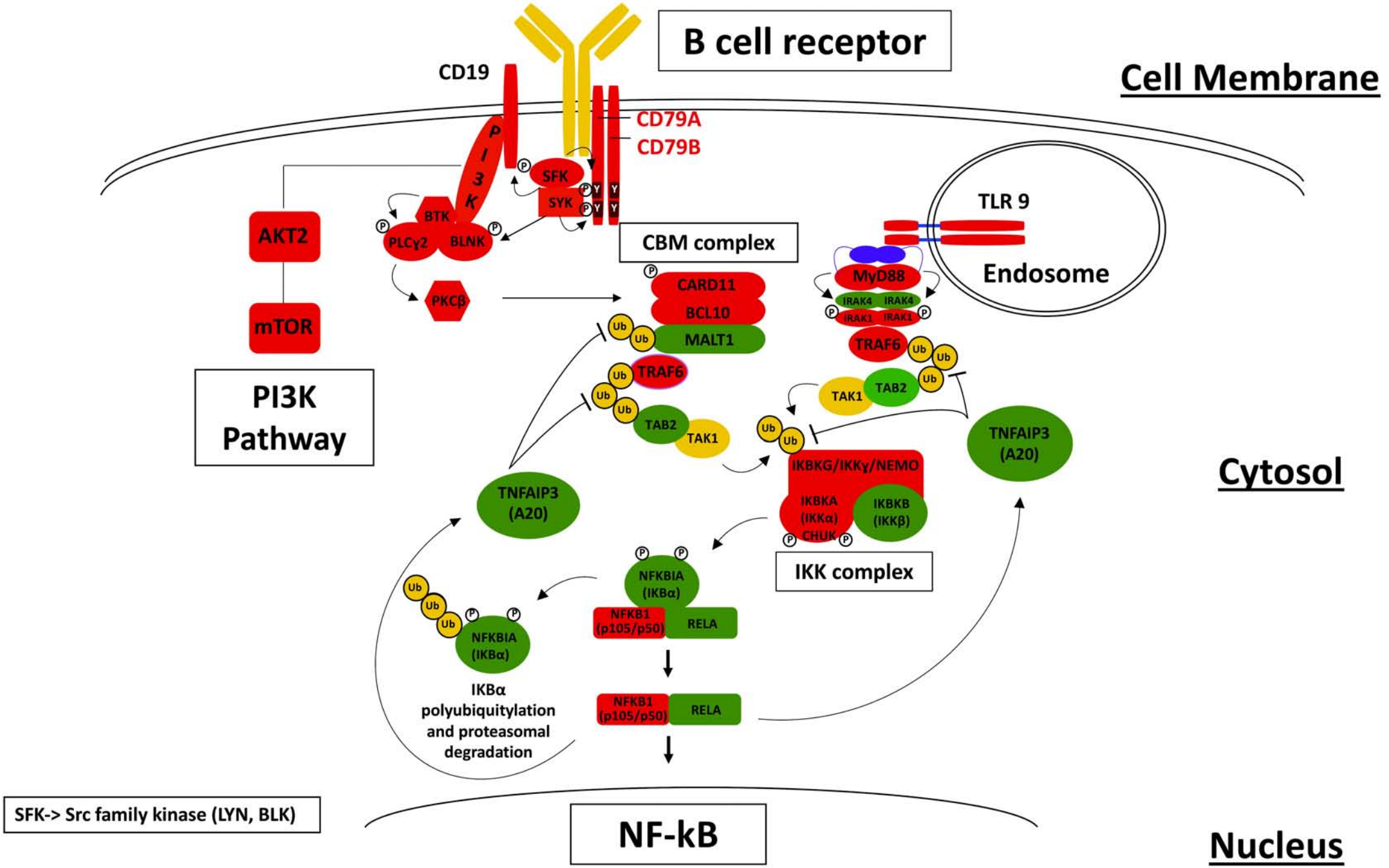
B cell receptor
Cell Membrane
CD19
CD79A
CD79B
PI3K
SFK
SYK
BTK
PLCγ2
BLNK
AKT2
mTOR
PI3K Pathway
PKCβ
CBM complex
CARD11
BCL10
MALT1
TRAF6
TAB2
TAK1
TLR 9
Endosome
MyD88
IRAK4
IRAK1
TRAF6
TAK1
TAB2
TNFAIP3 (A20)
IKBKG/IKKγ/NEMO
IKBKA (IKKα)
CHUK
IKBKB (IKKβ)
IKK complex
TNFAIP3 (A20)
NFKBIA (IKBα)
NFKB1 (p105/p50)
RELA
IKBα polyubiquitylation and proteasomal degradation
NFKB1 (p105/p50)
RELA
Cytosol
NF-kB
Nucleus
SFK-> Src family kinase (LYN, BLK)

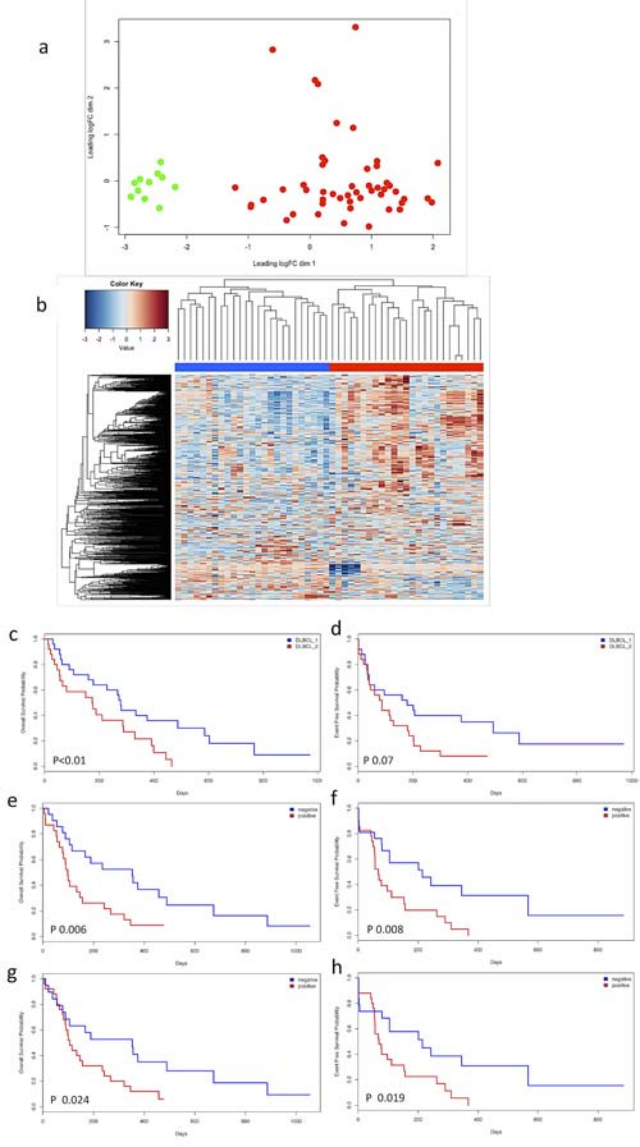
a
Leading logFC dim 2
Leading logFC dim 1
b
Color Key
Value
c
P<0.01
d
P 0.07
e
P 0.006
f
P 0.008
g
P 0.024
h
P 0.019

New molecular and therapeutic insights into canine diffuse large B cell lymphoma elucidates the role of the dog as a model for human disease

Luca Aresu [1*], Serena Ferraresso [2], Laura Marconato [3], Luciano Cascione [4,5], Sara Napoli [4], Eugenio Gaudio [4], Ivo Kwee [4,5,6], Chiara Tarantelli [4], Andrea Testa [7], Chiara Maniaci [7,8], Alessio Ciulli [7], Petra Hillmann [9], Thomas Bohnacker [10], Matthias P. Wymann [10], Stefano Comazzi [11], Massimo Milan [2], Fulvio Riondato [1], Giulia Dalla Rovere [2], Mery Giantin [2], Diana Giannuzzi [2], Francesco Bertoni [4*]

[1] Dipartimento di Scienze Veterinarie, Università degli Studi di Torino, Torino, Italy;
[2] Dipartimento di Biomedicina Comparata e Alimentazione, Università degli Studi di Padova, Padova, Italy;
[3] Centro Oncologico Veterinario, Sasso Marconi, Italy;
[4] Università della Svizzera italiana (USI), Institute of Oncology Research (IOR), Bellinzona, Switzerland;
[5] Swiss Institute of Bioinformatics (SIB), Lausanne, Switzerland;
[6] Dalle Molle Institute for Artificial Intelligence (IDSIA), Manno, Switzerland;
[7] Division of Biological Chemistry and Drug Discovery, School of Life Sciences, University of Dundee, Dundee, Scotland, United Kingdom;
[8] Department of Chemistry, Chemistry Research Laboratory, University of Oxford, Oxford, England, United Kingdom;
[9] PIQUR Therapeutics AG, Basel, Switzerland;
[10] Department of Biomedicine, University of Basel, Basel, Switzerland;
[11] Dipartimento di Medicina Veterinaria, Università degli Studi di Milano, Milano, Italy.

Online Supplementary Methods

DLBCL cohort of primary samples

Dogs with newly diagnosed, previously untreated, multi-centric DLBCL of any World Health Organization (WHO) clinical stage admitted to the Centro Oncologico Veterinario (Sasso Marconi, Italy) were included in the study. To be eligible for enrollment, dogs were required to undergo a complete staging work-up, consisting of history and physical examination, complete blood cell count with differential, serum biochemistry profile, thoracic radiographs and abdominal ultrasound, cytological evaluation of liver and spleen regardless of the ultrasonographic appearance, and immunophenotype determined by flow cytometry on a lymph node aspirate, peripheral blood and bone marrow aspirate. Before the initiation of therapy, all dogs underwent lymphadenectomy to confirm DLBCL histotype by routine histology and immunohistochemistry (CD3, CD20, CD79 and PAX5) and to provide material for the vaccine generation [1]. A portion of the neoplastic lymph node was always RNA-later preserved and stored at -80°C. In addition to tumor samples, skin punch biopsies were obtained from all the dogs included in the study to provide matched paired normal tissue. Dogs' owners were required to give written informed consent. Approval for this study was granted by the Ministero dell'Istruzione, dell'Universita' e della Ricerca Ethical Board (Number RBSI14EDX9).

Dogs comprised 39 (78%) purebred and 11 (22%) crossbred dogs; among the 39 purebred dogs, the three more frequent were German shepherds (*N* 7), Golden retrievers (*N* 4) and Rottweiler (*N* 3). There were 26 (52%) males (of which four were castrated), and 24 (48%) females (of which 15 were spayed). The median age was 7.5 years (range 3-15 years) and the median weight was 28.9 kg (range 4.5-81.3 kg). Based on the WHO staging system, two (4%) dogs had stage III disease, 15 (30%) had stage IV disease, and 32 (64%) had stage V disease. Among dogs with stage V disease, 25 (78.1%) dogs had PB and BM involvement, eight (41.2%) dogs had BM involvement, and one dog had PB involvement. Forty-three (86%) dogs had no symptoms at presentation (substage a), whereas 17 (14%) did (substage b). Twenty-six (52%) dogs had an increased LDH activity. Overall, 14 (28%) dogs received prednisone at a dose of 0.5-1.0 mg/kg before being referred. Thirty (60%) dogs were treated by means of a CHOP-based protocol with the incorporation of APAVAC

immunotherapy, as previously described. Briefly, chemotherapy consisted of L-Asparaginase (week 1), Vincristine (week 2, 3, 4, 13), Cyclophosphamide (week 2, 13), Doxorubicin (week 7, 16), Lomustine (week 10, 19), and prednisone (week 1 through 20). Dogs also received an intradermal injection of an autologous vaccine on weeks 4, 5, 6, 7, 12, 16, 20, and 24. Twenty (40%) dogs were treated with CHOP-based chemotherapy only.

Control samples were derived from lymph nodes of 11 dogs that were clinically normal both at physical examination and blood profile. A portion of lymph nodes was snap frozen in O.C.T immediately after sampling. Five-micrometer thick frozen sections were obtained, stained with hematoxylin and eosin, and immunostained for CD20 and CD3 to guide the dissection. The follicular B-cell compartment was isolated by laser capture microdissection using the Arcturus PixCell II system. Both DNA and RNA were extracted as follow.

The second independent series of 44 cDLBCLs comprised 30 (68%) purebred and 14 (32%) crossbred dogs; among the 30 purebred dogs, the three more frequent were Labrador retrievers (*N* 8), Golden retrievers (*N* 5) and Dogo Argentino (*N* 4). There were 22 (50%) males (of which six were castrated), and 22 (50%) females (of which 20 were spayed). The median age was 9 years (range 4-14 years) and the median weight was 26-7 kg (range 6.5-70.5 kg). Based on the WHO staging system, one (2%) dog had stage III disease, 20 (45%) had stage IV disease, and 23 (52%) had stage V disease. All the dogs were treated by means of a CHOP-based protocol with the incorporation of APAVAC immunotherapy,

RNA/DNA isolation and sequencing

Total RNA and DNA were extracted from all the samples, using the AllPrep DNA/RNA Mini Kit (Qiagen, Hilden, Germany) according to the manufacturer's instructions. DNA concentration and quality were measured by Qubit fluorometer (Life Technologies Ltd, Paisley, UK) and Agarose gel electrophoresis. While RNA concentration and integrity were measured in a NanoDrop ND-1000 spectrophotometer and assessed through the Bioanalyzer 2010 instrument (Agilent Technologies, Palo Alto, CA, USA).

A total of 61 non-normalized libraries for RNA sequencing experiments were prepared by using SureSelect Strand Specific RNA-Seq Library Preparation kit (Agilent Technologies) and a single end sequencing (50SE) was carried out on an Illumina HiSeq2500 (Illumina Inc., San Diego, CA, USA). Raw Illumina sequencing data are deposited on SRA database (GenBank) under accession numbers SRP137798. All Illumina reads were analyzed with FastaQC software in order to assess sequence quality.

Array Comparative Genomic Hybridization

In total, the DNA obtained from 50 cDLBCL specimens paired with normal counterpart were analyzed using a 180,000-feature SurePrint G3 Canine CGH Microarray (4x180K, Agilent Technologies), as previously described [2]. Raw and normalized fluorescence data of all microarray experiments have been deposited in the GEO database (www.ncbi.nlm.nih.gov/geo/) under accession number GSE113258.

Methyl-CpG-binding (MBD) sequencing

Both for cDLBCLs and controls, methylated DNA was enriched by the MethylMiner Methylated DNA Enrichment Kit (Life Technologies) according to manufacturer's instructions. Briefly, 2 µg of genomic DNA was sonicated, using Covaris S2 (Covaris, MA, USA), to obtain fragments ranging from 200 to 600 bp in size and captured by MBD proteins. The methylated fraction of genomic DNA (100 ng) thus obtained was then employed to construct barcoded DNA libraries by using the TruSeq Nano DNA LT Library Prep Kit (Illumina Inc.) and sequenced with HiSeq2500 instrument (Illumina Inc.) following a 50 SE approach. Raw Illumina sequencing data are deposited on SRA database (GenBank) under accession numbers SRP137788.

Immunohistochemical score

For PD-L1 and CTLA-4, immunohistochemical scoring was recorded as the percentage of positive tumor cells over total tumor cells in the denominator (TPS), as reported by Roach et al. [3]. PD-L1 expression was only considered when positive on the membrane of neoplastic lymphocytes. PD-L1

surface membrane expression detected on macrophages and small lymphocytes infiltrating the tumor was not considered. For PD-1 and CD5, tumor infiltrating lymphocytes positive labeled were counted using Image Pro-Plus software after low-magnification scansion of 10 representative fields at magnification x400. The result was expressed as the average of positive cells/x400. For statistical analysis a 50% cut-off TPS for PD-L1 and CTLA-4 immunohistochemical results was used. While for PD-1 and CD5, DLBCLs were classified as having either less than or more than 30 positive tumor infiltrating lymphocytes/x400 field.

Data Mining

RNA-Seq raw reads from library sequencing were mapped to the CanFam3.1 genome assembly (Broad Institute, Cambridge, MA; released Sep. 2011; downloaded from the Ensemble Genome Browser site) using the software tool STAR [4]. Next, we obtained counts of aligned reads per gene using htseq-count from the HTSeq software package [5] in single-stranded mode, with canine gene annotations from Ensembl Release 87. Only reads that were uniquely aligned were retained. Differential expression analysis was performed using EdgeR. Deregulated expression of genes was considered as significant when $p<0.05$ (FDR corrected) was observed. To find sources of similarity in the dataset consisting of all 61 samples and the expression values of expression-filtered genes, multidimensional scaling (MDS) was applied. In the analysis, hierarchical clustering was used [6]. The stability of the identified clusters was assessed using consensus clustering [7]. To identify functional categories of differentially expressed genes, Gene Set Enrichment Analysis (GSEA) [8] was performed using the Java GSEA implementation. MBD-seq sequence reads were aligned to the CanFam3.1 genome (Ensembl Release 87) using Bowtie2 [9]. Quality and validity check of the mapped methylation-CpG binding reads was performed and high quality sequence data (MPS≥10) were analyzed using the MEDIPS software package to estimate methylation levels [10]. We calculated the short read coverage (extend value=300) at genome-wide 100-bp bins. Differential methylation analysis was carried out in 300 bp windows excluding regions with no read coverage. Genomic regions with at least one consecutive window that were statistically significantly differentially methylated ($p\leq0.001$) between compared samples were considered to be differentially methylated regions (DMRs). DMRs were annotated to the canine genome with respect to gene features using HOMER annotatePeaks script. If a peak had two or more annotations, a priority was assigned based on the order from left to right.

Copy number variations (CNVs) data were analyzed as previously described [2]. The comparison of transcriptomes with CNVs was done using a modified GEDI algorithm as previously described by Lenz et al. [11]. Deletions in Chr 26 and Chr 17, detected in 41 and 40 dogs out of 50 dogs, respectively, and concurrent in 33 animals, encompassed the IGLλ and IGLK genes. Deletions in Chr 8, seen in 35 dogs, encompassed the *IGHV* gene. Since these three recurrent aberrations likely reflected the normal immunoglobulin genes rearrangement they were discarded for further analyses. The impact of deletions, gains and amplifications of the selected genes on their own expression level was evaluated by comparing the average gene expression levels of deleted, duplicated and normal samples using Student's t-test. To assess the correlation between RNA-Seq and MBD-seq, the correlation coefficient r was calculated and normalized to stabilize variance by applying Fisher's Z-transformation [12].

Overall survival (OS) was defined as the time from diagnosis to death. Event-free survival (EFS) was defined as the time from starting therapy to the date of any diagnosed relapse. Chi-square method was used for categorical variables and Student's T-test for continuous variables. Survival was estimated with the Kaplan-Meier method and compared by log-rank tests. P values less than 0.05 were considered statistically significant. Multivariate Cox regression analysis was used to assess the independent prognostic impact of different variables in terms of EFS and OS. The P values for multiple comparisons were adjusted using the Benjamini–Hochberg correction. Statistical analyses were carried out with R software v3.1.3.

Cell lines, small interfering RNAs and cell transfection

CLBL-1 cell line was kindly provided by Dr Barbara Rutgen (University of Wien). CLBL-1 was maintained in IMDM 10% FBS. Rational siRNA design was performed by Sfold, which consider

target accessibility and RNA duplex thermodynamics. The siRNAs were purchased from Ambion (Thermo Fisher Scientific) and sequences are shown in Table S8. Cells were electroporated with 200 pmol of each siRNAs using Nucleofector in SG solution and the protocol DS142 was chosen. Nucleofection efficiency was checked by FACS after 24h electroporation by fluorescent labelled control siRNA, BLOCK IT (200 pmol). Propidium iodide was used to check cell viability. RNA was extracted at 24h, 48h and 72h.

Reverse-Transcriptase Polymerase Chain Reaction (RT-PCR)

CLBL-1 total RNA was purified by phenol:chloroform extraction. RNA was also treated with DNase I (Qiagen) to remove genomic DNA. Quantitative RT-PCR (qRT-PCR) was performed using Qiagen One-Step RT-PCR kit (Qiagen) on ABI Step One Plus (Applied Biosystems) and primers for LIN28B and MYC indicated in *Online Supplementary Table S8*. qRT-PCR data were analyzed using $\Delta\Delta$Ct and normalized. The housekeeping CCZ1 was used as reference gene [13].

MTT proliferation assay

CLBL-1 was exposed to increasing doses of compounds as previously described [14]. Bimiralisib was kindly provided by Piqur Therapeutics (Basel, Switzerland), MZ1 was synthesized as previously described [15] and the other compounds were acquired from Selleck Chemicals (Houston, TX). Total RNA was extracted at different time points.

***In vivo* experiment**

Fifteen NOD-Scid (NOD.CB17-Prkdcscid/NCrHsd) mice were purchased from Harlan Laboratory (five-six weeks of age, approximately 20 g body weight). Mice maintenance and animal experiments were performed under institutional guidelines established for the Animal Facility of the Institute of Research in Biomedicine (Bellinzona, Switzerland) and with study protocols approved by the local Cantonal Veterinary Authority. Mice were subcutaneously engrafted with of the canine lymphoma cell line CLBL-1 (10 x10^6 cells in 0.1mL of PBS) and divided into three experimental groups. Starting with an average tumor volume of 40 mm3, mice underwent treatment with bimiralisib and with MZ1 while controls received vehicle only. Bimiralisib was prepared in 20% SBECD (sulfobutyl-ether-β-cyclodextrin, Captisol, Dexolve) in water and pH was adjusted to 3.1. Application volume was 10 mL/kg and mice received through oral gavage (p.o.) 100 mg/Kg of bimiralisib every day for one week. MZ1 was prepared in 25% HP-ß-CD [(2-Hydroxypropyl)-β-cyclodextrin; Sigma Aldrich, MO, USA] in water and pH was adjusted to 6.2. Application volume was 5 mL/kg and mice were injected intraperitoneally (i.p.) with 100 mg/Kg of MZ1 every day for one week. Tumor size was measured as previously described [16].

Immunohistochemistry

Paraffin blocks obtained by formalin fixed tumor samples were cut into 5 µm sections on superfrost slides. Briefly, slides were placed in 70°C paraffin oven for 1 hour before deparaffinized in xylene and then rehydrated in 100%, 90%, 70% alcohol, successively. Antigen was retrieved by citric acid buffer (pH 6.0) in the 95°C water bath for 20 minutes. Endogenous peroxidase was inactivated by incubation in 3% H2O2 for 15 minutes. Following a pre-incubation with 10% normal goat serum to block nonspecific sites for 30 minutes, the sections were incubated with primary antibodies at room temperature for 30 minutes (anti-bovine PD-L1 monoclonal antibody, 5A2-A1, was diluted with PBS at 1:100, goat polyclonal anti-PD1 antibody, ab36151, at 1:100, mouse monoclonal anti-CTLA-4, ANC152.2, at 1:100, and mouse monoclonal anti-CD5, YKIX322.3, at 1:50). After the sections were washed with PBS twice for 5 minutes, positive staining was visualized with 3-diaminobenzidine tetrahydrochloride (DAB) according to manufacturer's protocol.

ONLINE SUPPLEMENTARY REFERENCES

1. Marconato L, Frayssinet P, Rouquet N, et al. Randomized, placebo-controlled, double-blinded chemoimmunotherapy clinical trial in a pet dog model of diffuse large B-cell lymphoma. Clin Cancer Res. 2014;20(3):668-677.
2. Arico A, Ferraresso S, Bresolin S, et al. Array-based comparative genomic hybridization analysis reveals chromosomal copy number aberrations associated with clinical outcome in canine diffuse large B-cell lymphoma. PLoS One. 2014;9(11):e111817.

3. Roach C, Zhang N, Corigliano E, et al. Development of a Companion Diagnostic PD-L1 Immunohistochemistry Assay for Pembrolizumab Therapy in Non-Small-cell Lung Cancer. Appl Immunohistochem Mol Morphol. 2016;24(6):392-397.
4. Dobin A, Davis CA, Schlesinger F, et al. STAR: ultrafast universal RNA-seq aligner. Bioinformatics. 2013;29(1):15-21.
5. Anders S, Pyl PT, Huber W. HTSeq--a Python framework to work with high-throughput sequencing data. Bioinformatics. 2015;31(2):166-169.
6. Eisen MB, Spellman PT, Brown PO, Botstein D. Cluster analysis and display of genome-wide expression patterns. Proc Natl Acad Sci U S A. 1998;95(25):14863-14868.
7. Monti S, Savage KJ, Kutok JL, et al. Molecular profiling of diffuse large B-cell lymphoma identifies robust subtypes including one characterized by host inflammatory response. Blood. 2005;105(5):1851-1861.
8. Subramanian A, Tamayo P, Mootha VK, et al. Gene set enrichment analysis: a knowledge-based approach for interpreting genome-wide expression profiles. Proc Natl Acad Sci U S A. 2005;102(43):15545-15550.
9. Langmead B, Salzberg SL. Fast gapped-read alignment with Bowtie 2. Nat Methods. 2012;9(4):357-359.
10. Weber M, Davies JJ, Wittig D, et al. Chromosome-wide and promoter-specific analyses identify sites of differential DNA methylation in normal and transformed human cells. Nat Genet. 2005;37(8):853-862.
11. Lenz G, Wright GW, Emre NC, et al. Molecular subtypes of diffuse large B-cell lymphoma arise by distinct genetic pathways. Proc Natl Acad Sci U S A. 2008;105(36):13520-13525.
12. Woo HG, Choi JH, Yoon S, et al. Integrative analysis of genomic and epigenomic regulation of the transcriptome in liver cancer. Nat Commun. 2017;8(1):839.
13. Giantin M, Aresu L, Arico A, et al. Evaluation of tyrosine-kinase receptor c-KIT (c-KIT) mutations, mRNA and protein expression in canine leukemia: might c-KIT represent a therapeutic target? Vet Immunol Immunopathol. 2013;152(3-4):325-332.
14. Boi M, Gaudio E, Bonetti P, et al. The BET Bromodomain Inhibitor OTX015 Affects Pathogenetic Pathways in Preclinical B-cell Tumor Models and Synergizes with Targeted Drugs. Clin Cancer Res. 2015;21(7):1628-1638.
15. Zengerle M, Chan KH, Ciulli A. Selective Small Molecule Induced Degradation of the BET Bromodomain Protein BRD4. ACS Chem Biol. 2015;10(8):1770-1777.
16. Tarantelli C, Gaudio E, Arribas AJ, et al. PQR309 Is a Novel Dual PI3K/mTOR Inhibitor with Preclinical Antitumor Activity in Lymphomas as a Single Agent and in Combination Therapy. Clin Cancer Res. 2018;24(1):120-129.
17. Charoentong P, Finotello F, Angelova M, et al. Pan-cancer Immunogenomic Analyses Reveal Genotype-Immunophenotype Relationships and Predictors of Response to Checkpoint Blockade. Cell Rep. 2017;18(1):248-262.

SUPPLEMENTARY TABLES

Supplementary Table S1. Differential expression analysis between cDLBCLs and normal lymph nodes. Columns A-C: Dog gene IDs (Ensembl and Entrez) and gene symbols. Column D: Gene type. Columns E,F: corresponding human gene IDs and gene symbols. Column G: likelihood ratio (LR) statistics. Column H: average logCPM (count-per-million) across all samples. Column I: logFC (Fold-change) between cDLBCLs and normal lymph nodes. Columns J-K: nominal and BH-adjusted (FDR) p-value.

Supplementary Table S2. Differential expression analysis between CLBL-1 cell line and normal lymph nodes. Columns A-C: Dog gene IDs (Ensembl and Entrez) and gene symbols. Column D: Gene type. Columns E,F: corresponding human gene IDs and gene symbols. Column G: likelihood ratio (LR) statistics. Column H: average logCPM (count-per-million) across all samples. Column I: logFC (Fold-change) between CLBL-1 and normal lymph nodes. Columns J-K: nominal and BH-adjusted (FDR) p-value.

Supplementary Table S3. Genes found differentially expressed in chromosomal regions with aberrations (Gains and Losses). Columns A-B: Dog gene IDs (Ensembl) and gene symbols. Column C: logFC (Fold-change) between cDLBCLs and normal lymph nodes. Columns D: BH-adjusted (FDR) p-value. Column E: Gene type.

Supplementary Table S4. Regions found differentially methylated between cDLBCLs and normal B-cells. Table S5 contains four worksheets organized as follow: **S2.1** Genomic regions significantly hypomethylated in cDLBCL compared to normal lymph nodes; **S2.2** Gene Set Enrichment Analysis (GSEA) of hypomethylated genes; **S2.3** Genomic regions significantly hypermethylated in cDLBCL compared to normal lymph nodes; **S2.4** GSEA of hypermethylated genes.

Supplementary Table S5. Differential expression analysis between cDLBCL1 and cDLBCL2. Columns A-C: Dog gene IDs (Ensembl and Entrez) and gene symbols. Column D: Gene type. Columns E,F: corresponding human gene IDs and gene symbols. Column G: likelihood ratio (LR) statistics. Column H: average logCPM (count-per-million) across all samples. Column I: logFC (Fold-change) between cDLBCLs and normal lymph nodes. Columns J-K: nominal and BH-adjusted (FDR) p-value.

Supplementary Table S6. Univariate and multivariate Cox regression analysis of overall survival for PD-L1 and PD-1 immunohistochemistry.

	Univariate Analysis			Multivariate Analysis		
	HR	**95% CI**	**P value**	**HR**	**95% CI**	**P value**
PD-L1 negative	0.446	0.234-0.765	0.006	0.505	0.274-0.956	0.036
PD-L1 positive	1					
PD-1 negative	0.551	0.351-1.155	0.024	0.945	0.301-1.452	0.041
PD-1 positive	1					
Age (<10 years)	0.765	0.541-1.575	0.397			
Age (>10 years)	1					
Stage (1-4)	1.542	0.884-3.553	0.145			
Stage (5)	1					
Substage a	1.753	1.054-2.563	0.021	2.405	1.309-4.794	0.011
Substage b	1					
Bone Marrow Infiltration neg	1.899	1.452-2.463	0.014	2.422	1.804-2.941	0.021
Bone Marrow Infiltration pos	1					

Supplementary Table S7 Sequences of siRNAs targeting LIN28B and primer sequences for LIN28B and MYC gene expression analysis by qRT-PCR.

siRNA sequences

siRNA	SENSE STRAND	ANTISENSE STRAND
LIN28Bex3	GGAUUCAUCUCCAUGAUAATT	UUAUCAUGGAGAUGAAUCCTT
LIN28B ex4	UGAAUCAAUACGGGUAACUTT	AGUUACCCGUAUUGAUUCATT

LIN28B and MYC primer sequences

PRIMER	FORWARD	REVERSE
LIN28B	CCTTGGATATTCCAGTCGATGT	TGGTTCTCCTTCTTTTAGGCTTCTA
MYC	TCCTCGGACTCTCTGCTCTC	TCAATTTCTTCTTCGTCCTCTTG

SUPPLEMENTARY FIGURES

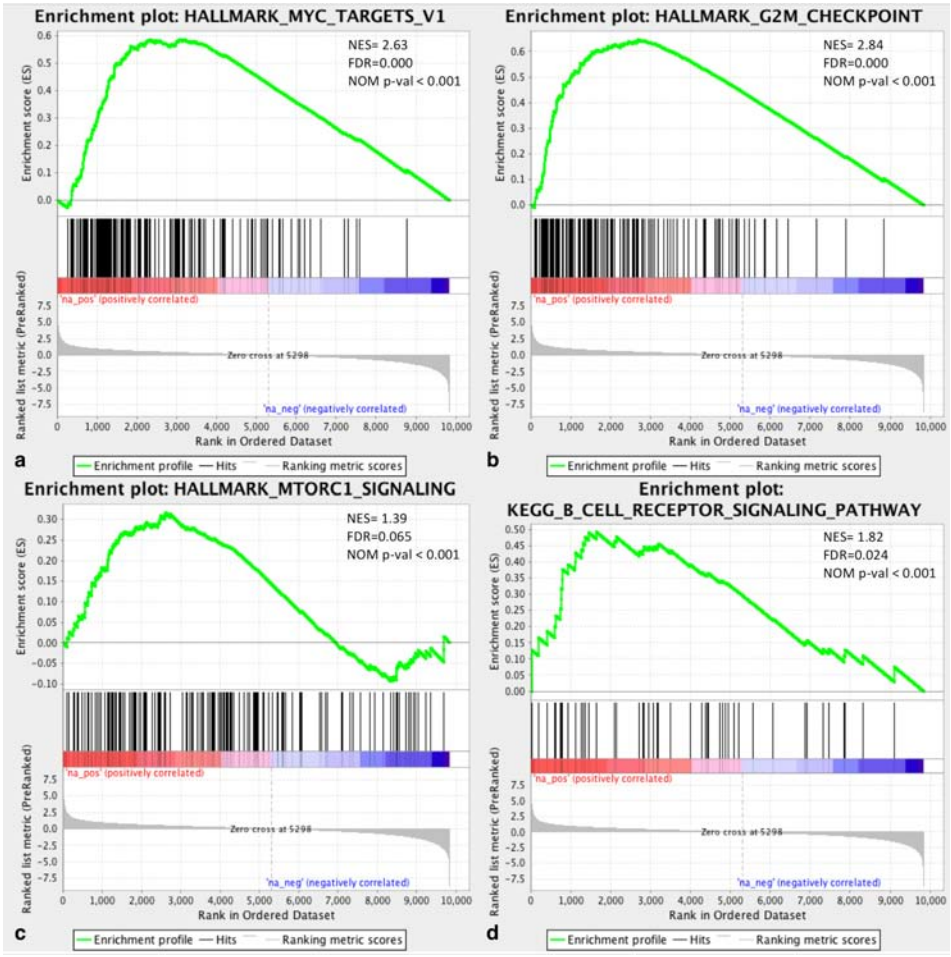

Supplementary Figure S1. GSEA plots for gene-expression signatures obtained in canine DLBCL compared to normal B-cells. Enrichment plots of MYC-targets **(a)**, G2M checkpoint **(b)**, MTORC1 signaling **(c)** and BCR signaling pathway **(d)**. Top, upregulated genes; bottom, downregulated genes. Green line, enrichment score; bars in the middle portion of the plots show where the members of the gene set appear in the ranked list of genes; Positive or negative ranking metric indicates, respectively, correlation or inverse correlation with the profile; NES, normalized enrichment score.

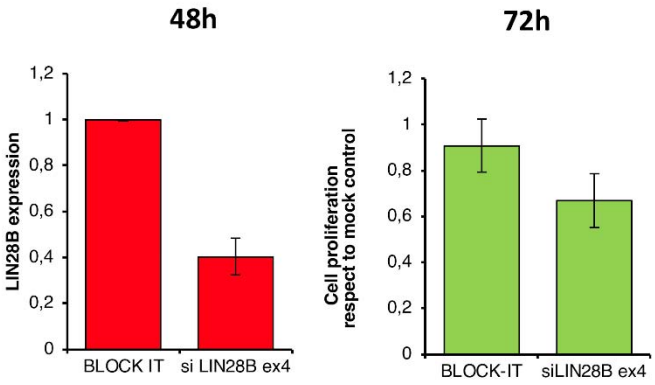

Supplementary Figure S2. LIN28B mRNA expression after 48h from transfection with LIN28B ex4 siRNA (*si LIN28B ex4*) compared to control (*BLOCK-IT*) (left panel). Cell viability after 72h from nucleofection with LIN28B ex4 siRNA (*si LIN28B ex4*) compared to control (*BLOCK-IT*) measured by MTT assay (right panel). Results are expressed as average of three independent experiments.

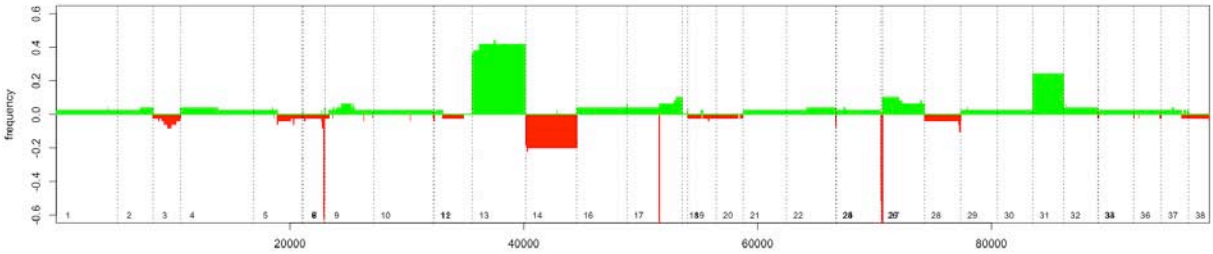

Supplementary Figure S3. **Frequency plots of DNA gains (green) and losses (red) observed in 50 canine DLBCLs.** X axis: chromosome localization and physical mapping. Y axis: percentage of cases bearing the aberration.

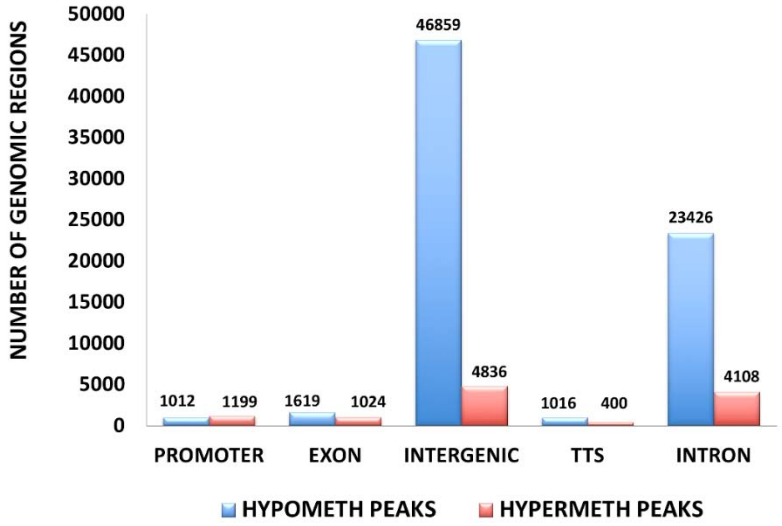

Supplementary Figure S4. Bar plots showing the number of differentially methylated peaks in canine DLBCL compared with normal B-cells. Results are reported separating peaks according to genomic locations.

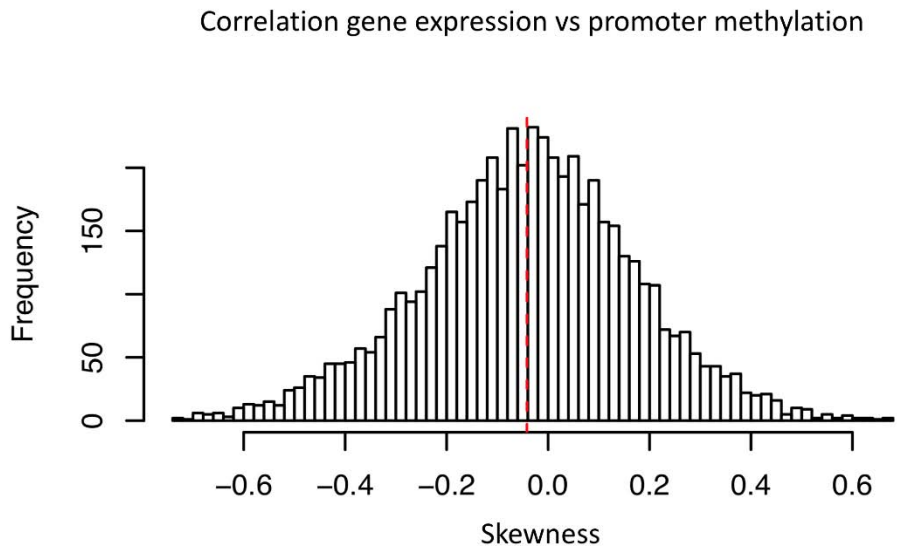

Supplementary Figure S5. Histogram and skewed distribution showing a negative correlation between the differences in mRNA expression and promoter methylation (skewness= -0.06, *P* <0.01). The red line represents a linear regression.

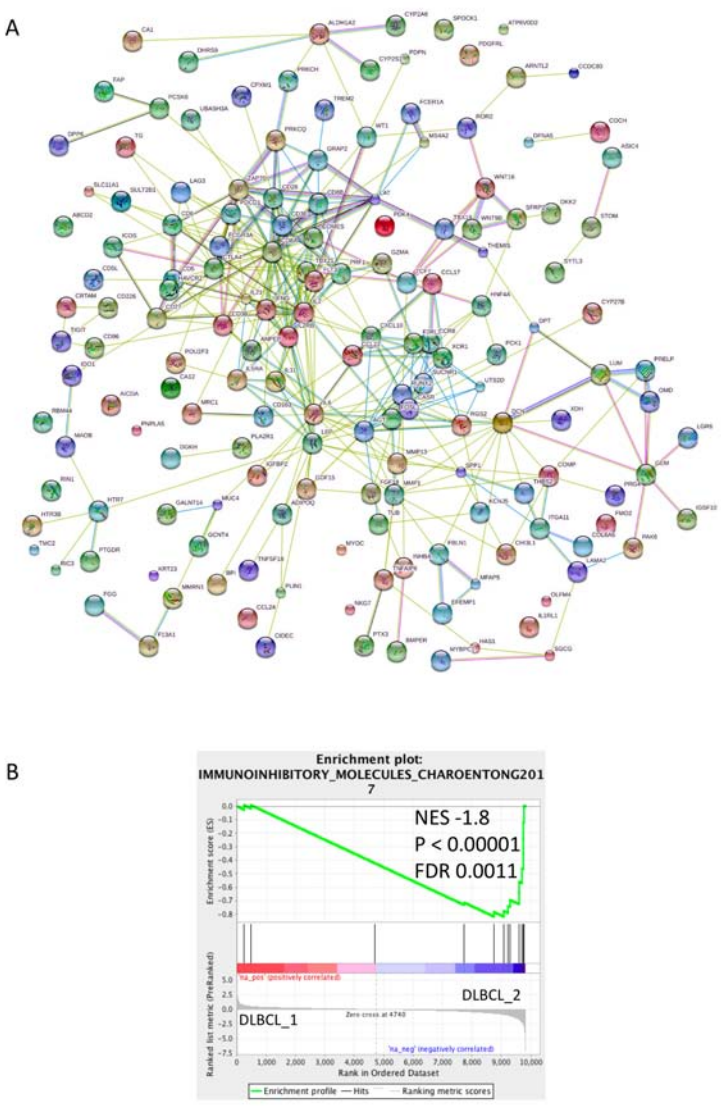

Supplementary Figure S6. Functional analysis of genes significantly up-regulated in DLBCL_2 compared to DLBCL_1. A. Representative protein-protein interaction network of genes generated from STRING database. The connecting lines indicate functional relationships and direct protein-protein interactions. B. GSEA plot for gene-expression signatures obtained in DLBCL_1 compared to DLBCL_2 and then analyzed for their enrichment in immunoinhibitory molecules as reported by Charoentong et al. [17]. Green line, enrichment score; bars in the middle portion of the plots show where the members of the gene set appear in the ranked list of genes; Positive or negative ranking metric indicates, respectively, correlation or inverse correlation with the profile; NES, normalized enrichment score.

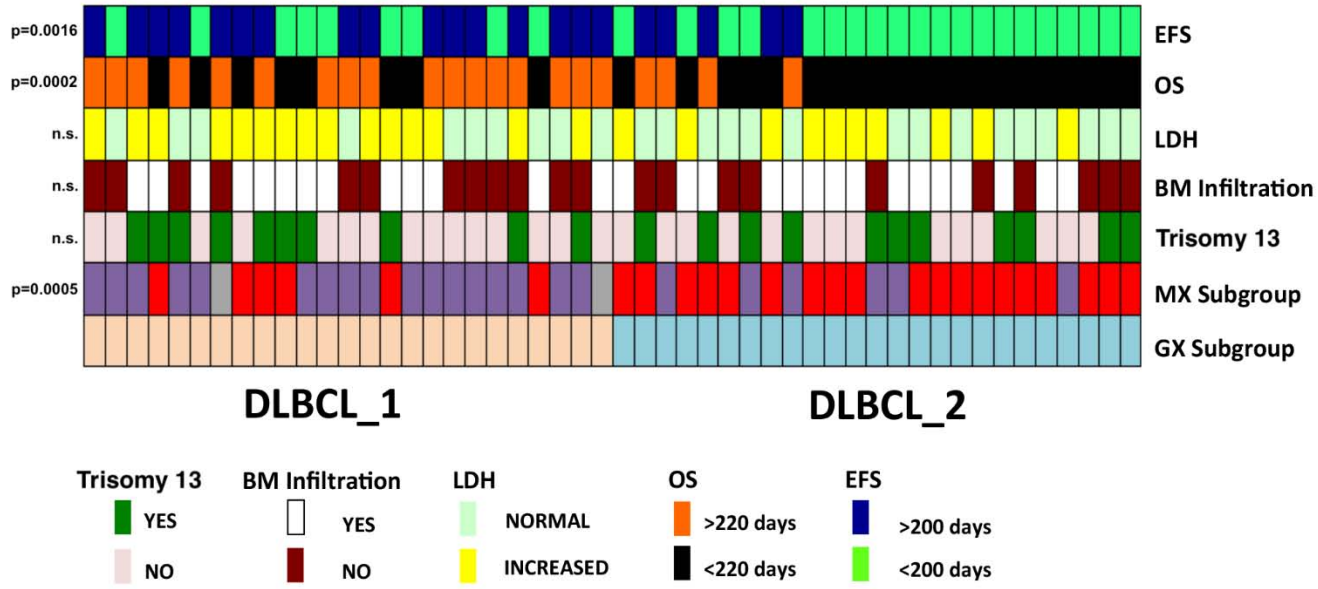

Supplementary Figure S7. Clinical, molecular and genotypic features of cDLBCLs. Tumor subgroups identified by RNA-seq (GX Subgroup) are indicated in salmon (DLBCL_1) and light blue (DLBCL_2) bars; methylation subgroups (MX Subgroup) obtained by unsupervised clustering are indicated in violet (group 1), red (group 2) and grey (group 3). Trisomy of chromosome 13, bone marrow (BM) infiltration, LDH, Overall Survival (OS) and Event Free Survival (EFS) in individual tumors are indicated. Significant correlation between clinical/molecular features and GX subgroups are reported on the left.

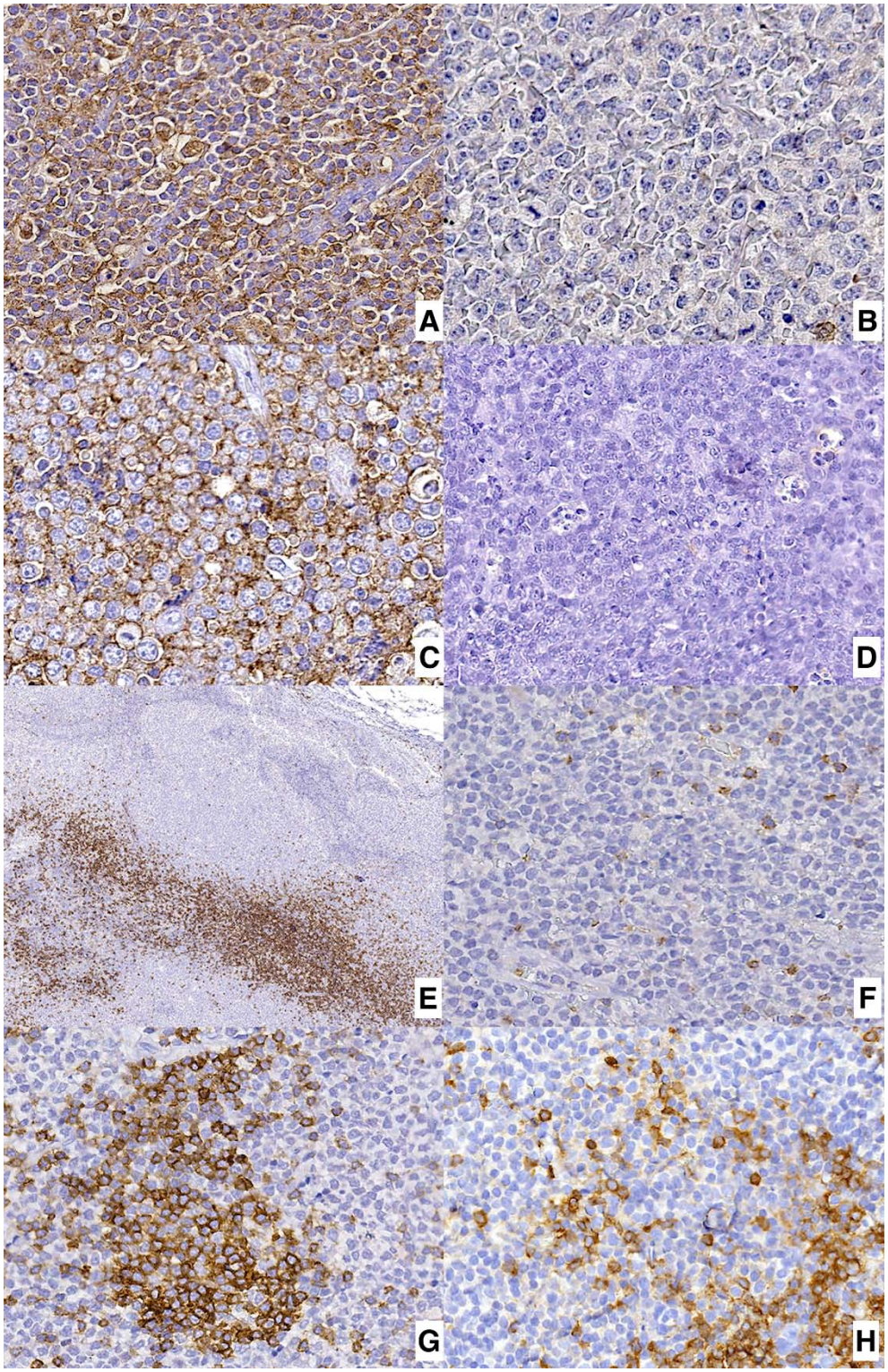

Supplementary Figure S8. Representative immunohistochemical analysis of PD-L1, CTLA-4, PD-1 and CD5 expression in cDLBCL. (A) PD-L1 positive tumor cells in cDLBCL. (B) PD-L1 negative tumor cells in cDLBCL. (C) CTLA-4 positive tumor cells in cDLBCL. (D) CTLA-4 negative tumor cells in cDLBCL. (E) PD-1 lymphocytes in cDLBCL. (F) Small number of PD-1 lymphocytes in cDLBCL. (G) CD5 lymphocytes in cDLBCL. (H) Small number of CD5 lymphocytes in cDLBCL.

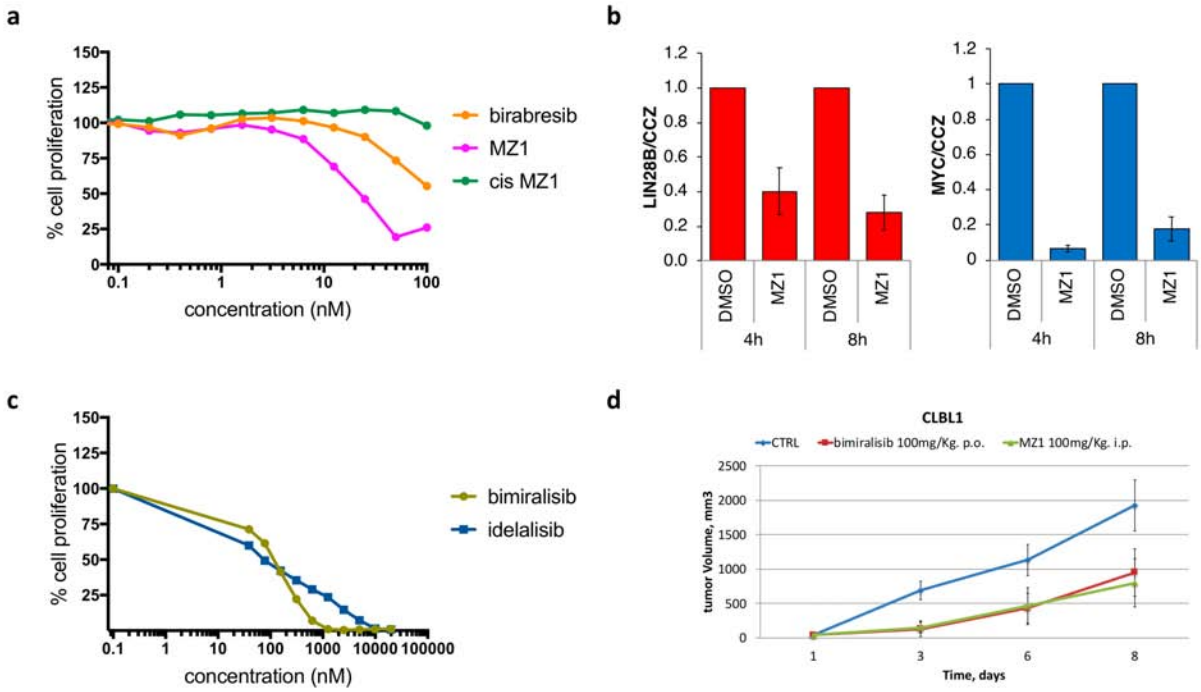

Supplementary Figure S9. Activity of targeted molecules on CLBL1 cell line. (a) CLBL1 cell line was exposed to increased doses of birabresib (OTX015/MK-8628), MZ1 or cis MZ1 for 72 hours. Anti-proliferative activity was evaluated by MTT assay. **(b)** CLBL1 cell line was treated with DMSO or MZ1 (500 nM) for 4 and 8 hours and expression of LIN28B (left) or MYC (right) was evaluated by Real Time-PCR. **(c)** CLBL1 cell line was exposed to increased doses of bimiralisib (PQR309) or idelalisib for 72 hours. Anti-proliferative activity was evaluated by MTT assay. Results are expressed as average of three independent experiments. **(d)** NOD-SCID mice subcutaneously inoculated with the CLBL-1 cell line and treated with bimiralisib (n = 5), with MZ1 (n = 5) or vehicle control (CTRL, n = 5). Y-axis: Tumor volumes in mm3. X-axis, days post first treatment (Day 1).

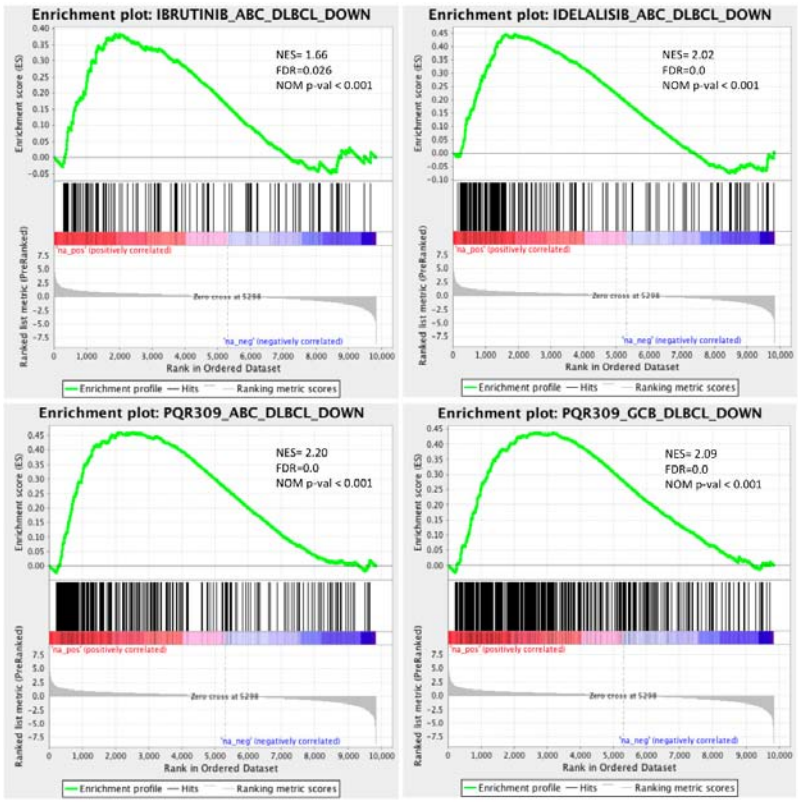

Supplementary Figure S10. GSEA plots for gene-expression signatures obtained in cDLBCL compared to controls and then analyzed for their enrichment in ibrutinib target genes (top left), idelalisib target genes (top right), and bimiralisib (PQR309) target genes in ABC-DLBCL (bottom left) as well as bimiralisib target genes in GC-DLBCL (bottom right), as defined by Tarantelli et al. [16]. Top, upregulated genes; bottom, downregulated genes. Green line, enrichment score; bars in the middle portion of the plots show where the members of the gene set appear in the ranked list of genes; Positive or negative ranking metric indicates, respectively, correlation or inverse correlation with the profile; NES, normalized enrichment score.